Cell Reports, Volume *14*

Supplemental Information

RAB-5- and DYNAMIN-1-Mediated Endocytosis of EFF-1 Fusogen Controls Cell-Cell Fusion

Ksenia Smurova and Benjamin Podbilewicz

Supplemental information for

RAB-5- and DYNAMIN-1-Mediated Endocytosis of EFF-1 Fusogen Controls Cell-Cell Fusion

Ksenia Smurova[1] and Benjamin Podbilewicz[1]*

[1]Department of Biology, Technion-Israel Institute of Technology, Haifa 32000, Israel
*Author for correspondence (podbilew@technion.ac.il)

This file includes:
Supplemental Figures S1-S5
Supplemental Figure legends S1-S5
Supplemental Tables S1-S3
Movie legends S1-S6
Supplemental experimental procedures
Supplemental references

Supplemental Figures

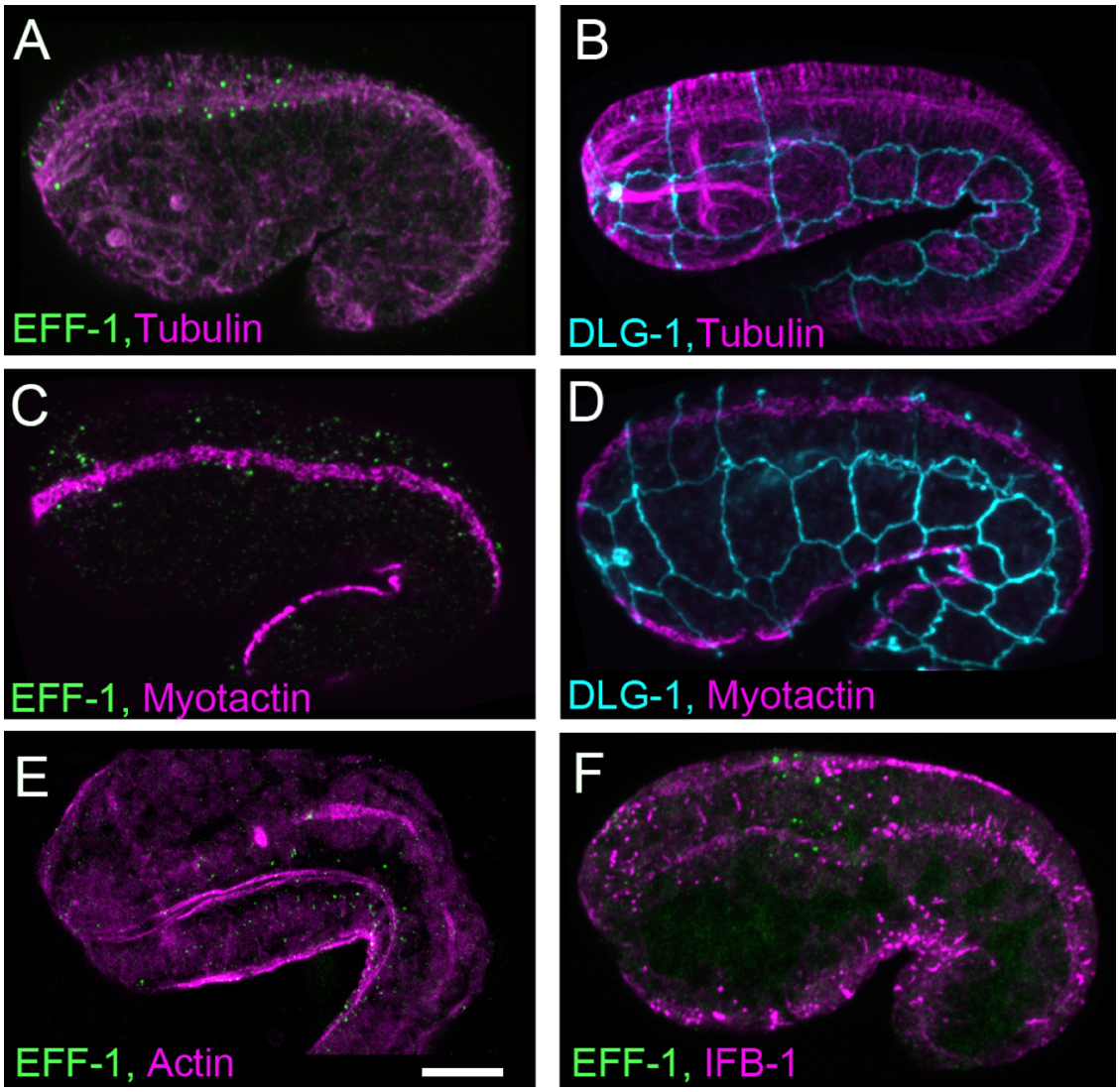

Figure S1. EFF-1 puncta arrangement along microtubule bundles, related to Figure 1
Organization of EFF-1 and cell junctions with respect to the cytoskeleton was analyzed by immunofluorescence. Scale bar, 10 μm.
(A) EFF-1 puncta along microtubule longitudinal bundles. Anti-EFF-1 antibody, green; anti-tubulin antibody, magenta.
(B) Bundles of microtubules localize parallel to the row of seam cells. Anti-tubulin antibody, magenta; anti-DLG-1 antibody, cyan.
(C) EFF-1 does not colocalize with fibrous organelles (hemidesmosome-like structures). Anti-EFF-1 antibody, green; anti-myotactin antibody, magenta.
(D) Fibrous organelles are aligned parallel to the row of seam cells. Anti-myotactin antibody, magenta; anti-DLG-1 antibody, cyan.
(E) EFF-1 does not colocalize with actin. Anti-EFF-1 antibody, green; Texas Red-phalloidin, magenta.
(F) Intermediate filaments do not show colocalization with EFF-1 puncta in embryos expressing IFB-1::GFP. Anti-EFF-1 antibody, green; anti-GFP antibody, magenta.

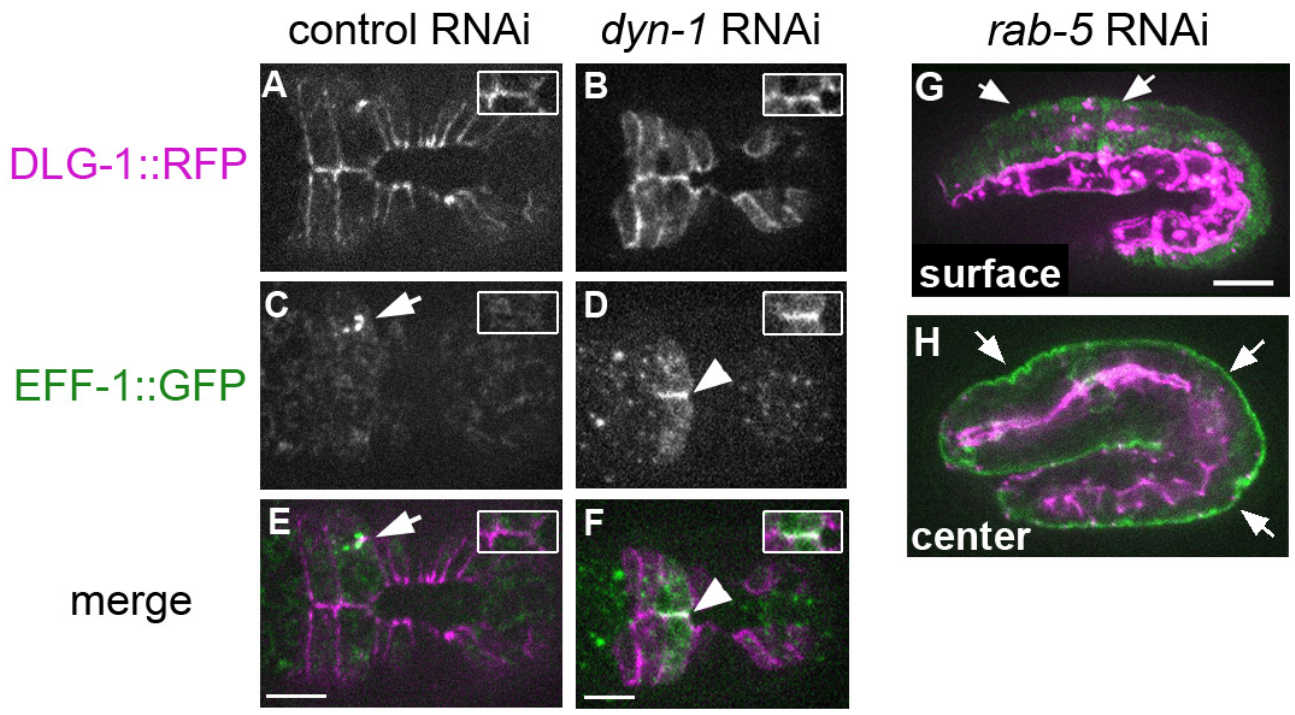

Figure S2. DYN-1 and RAB-5 knockdown induces EFF-1::GFP plasma membrane accumulation, related to Figure 2

(A-F) Ventral views of live embryos before the first fusion event under control RNAi and *dyn-1* RNAi treatment. Insets represent the areas of cell junctions between the cells in the process of fusion. EFF-1::GFP localize to cytoplasmic vesicles in control RNAi embryos (C, E, arrows). EFF-1::GFP shows plasma membrane mislocalization in *dyn-1* RNAi embryos (D, F arrowheads)

(G, H) EFF-1::GFP (green) and DLG-1::RFP (magenta) expression in *rab-5* RNAi treated embryos. Surface focus shows hyperfusion of hypodermal cells (G), center focus represents EFF-1 apical membrane localization (H, arrows; See also Movie S5). Scale bars, 10 μm.

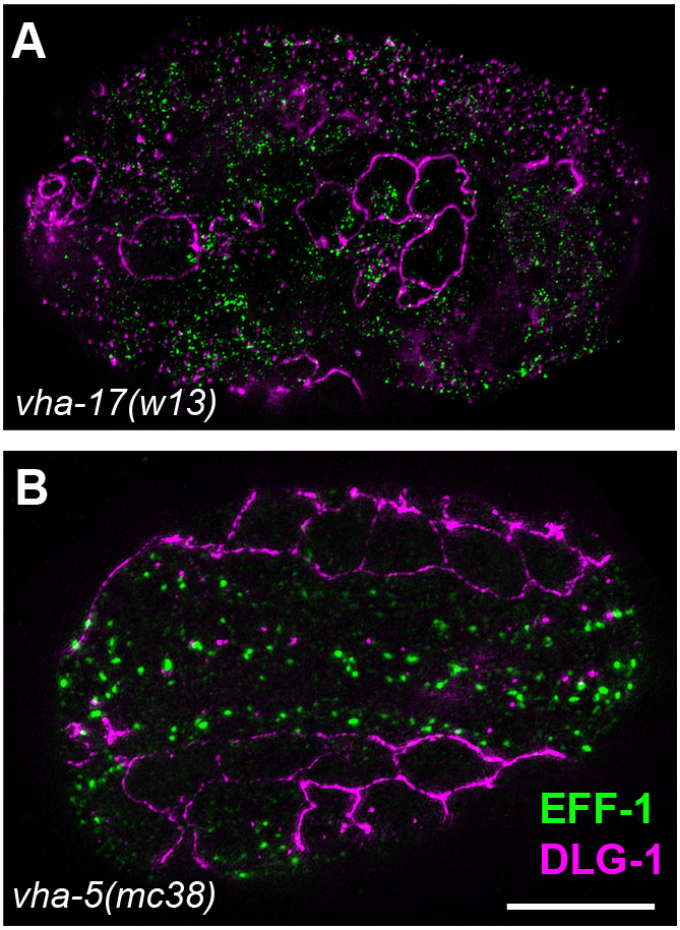

Figure S3. V-ATPase regulates cell fusion, related to Figure 3
Effect of mutations in two subunits of the vacuolar ATPase, VHA-17, and VHA-5, affect EFF-1 localization and fusion. Embryos were incubated at room temperature for 5-20 h and immunostained with anti-EFF-1 (green) and anti-DLG-1 antibody (magenta) followed SIM.
(A) Hyperfusion phenotype caused by *vha-17* mutation associates with smaller but denser EFF-1 puncta which did not colocalize with cell junctions.
(B) *vha-5* mutation induces hyperfusion but does not change EFF-1 localization.
Scale bar, 10 μm.

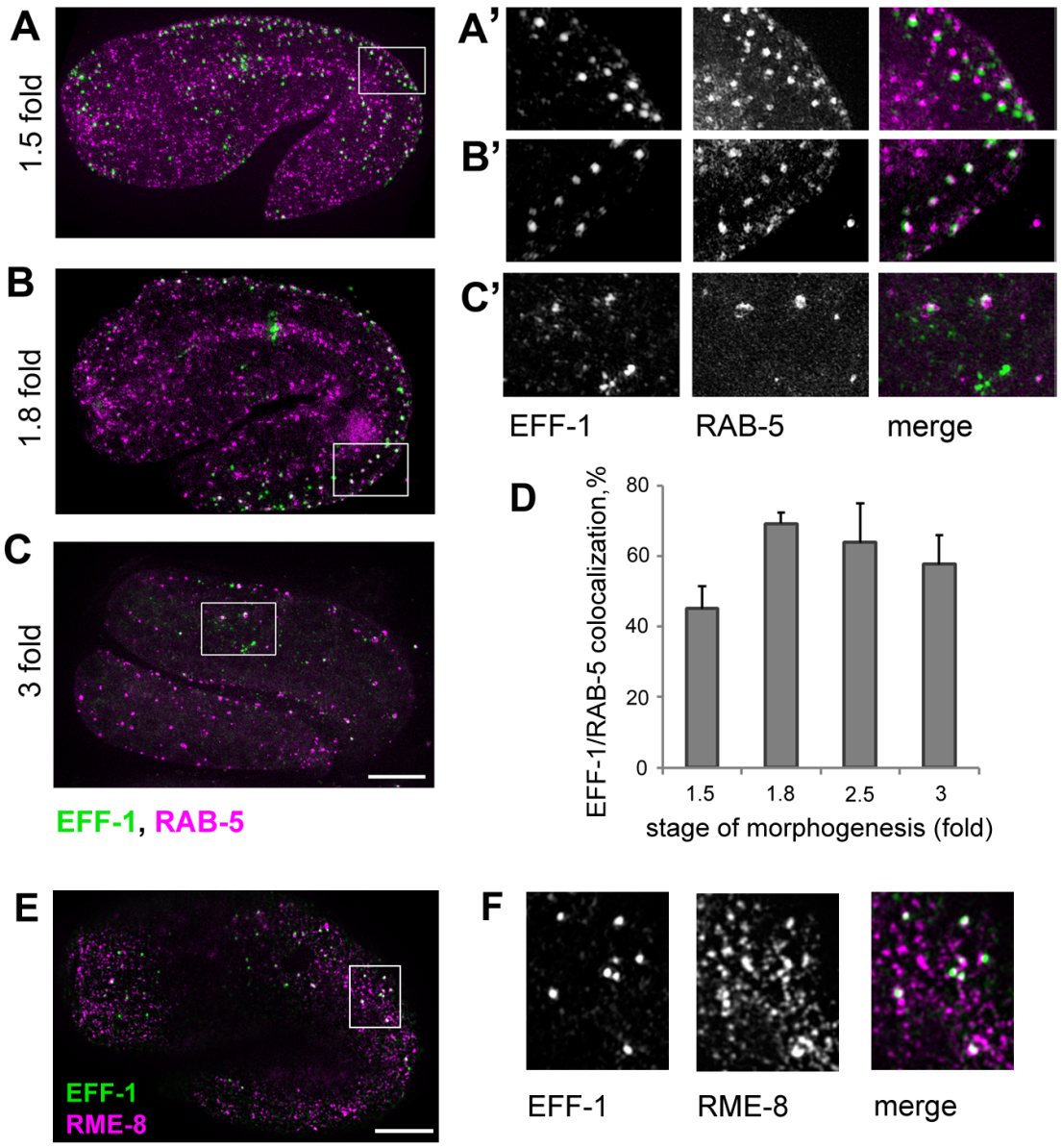

Figure S4. EFF-1/RAB-5 and EFF-1/RME-8 colocalization, related to Figure 4.
(A-C) EFF-1/RAB-5 colocalization changes in embryonic development. EFF-1 (green) and RAB-5 (magenta) colocalization at different stages of embryonic fusion was visualized by immunofluorescence with specific antibodies.
(A) 1.5 fold embryo
(B) 1.8 fold embryo
(C) 3 fold embryo
(A'-C') Enlargements of inset regions from (A-C) showing EFF-1, RAB-5 immunofluorescence, and merged images.
(D) Percentage of EFF-1 colocalization with RAB-5 during embryonic development (mean ± SEM). Number of puncta analyzed for each stage of morphogenesis was n>200.
(E) Colocalization of EFF-1 (green) with RME-8 (magenta, marker that is present in early, recycling, and late endosomes). EFF-1 and RME-8 patterns are visualized using immunofluorescence.
(F) Boxed region from (E) is enlarged and shown in separate channels: EFF-1, left; RME-8, middle; and merged, right.
Scale bars, 10 μm.

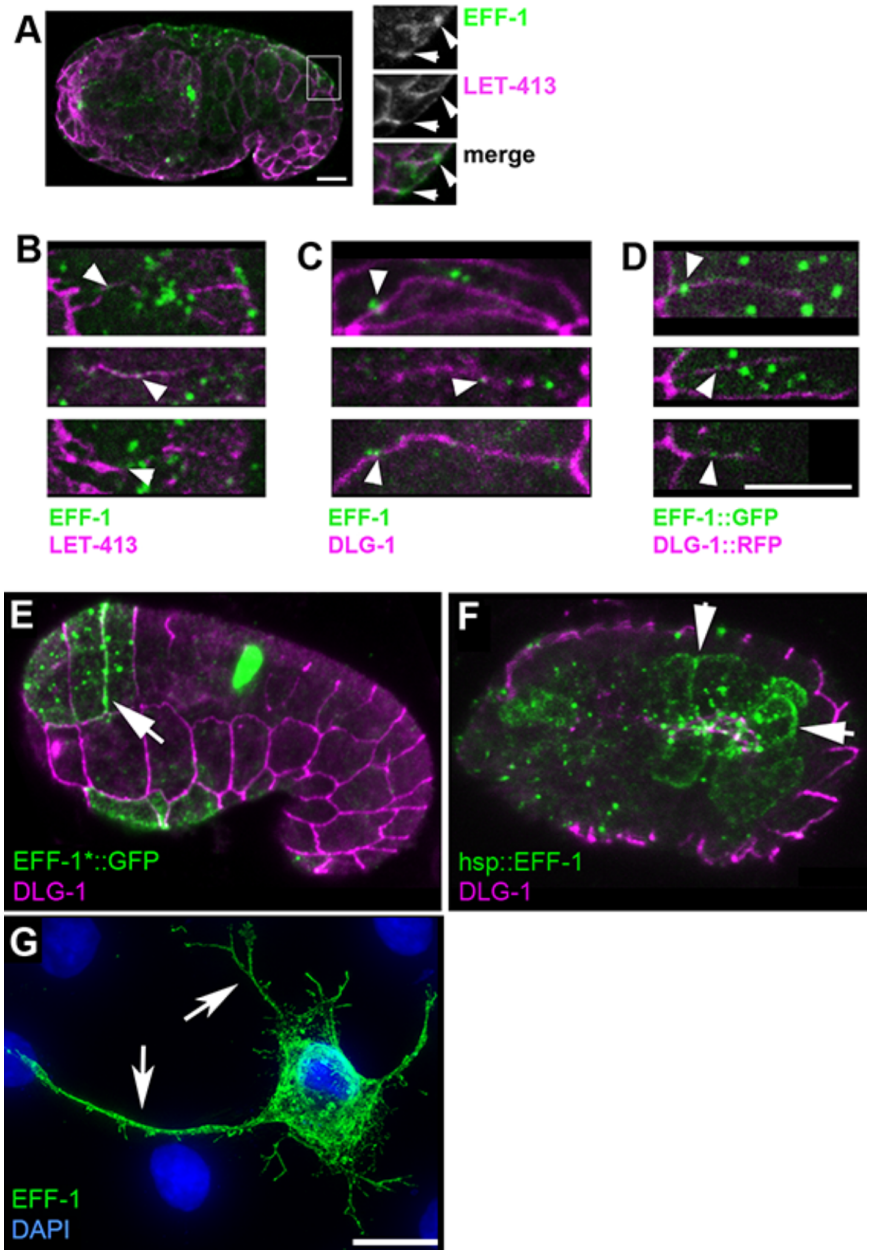

Figure S5. EFF-1 colocalization with membranes and apical junctions, related to Figure 6

(A) EFF-1 colocalization with basolateral membrane before fusion in LET-413::CFP expressing embryo is revealed by immunofluorescence with anti-EFF-1 (green) and anti-GFP antibody (LET-413, magenta).

(B-D) Individual confocal z-slices of cell junctions were taken from the dorsal side of embryos in the process of fusion. Enlarged areas of diverse junctions show partial EFF-1 colocalization with cell junctions (arrowheads).

(B) EFF-1 (green) and basolateral membrane marker LET-413::CFP (magenta) are visualized by immunofluorescence with anti-EFF-1 and anti-CFP antibody.

(C) Endogenous EFF-1 was immunolabled with anti-EFF-1 antibody, green; apical junctions were detected with anti-DLG-1 antibody, magenta.

(D) Live images of apical junctions (DLG-1::RFP, magenta) showing transient colocalization with EFF-1::GFP (green) prior to cell fusion.

(E) Nonfusogenic EFF-1::GFP* accumulation at the plasma membrane (arrow) in *C. elegans* embryo (*Del Campo et al., 2005). Immunofluorescence with anti-GFP antibody (green) and anti-DLG-1 (apical junction, magenta).

(F) Ectopic EFF-1 localization to the plasma membrane of intestinal cells (arrows) following heat shock in an embryo expressing *hsp::eff-1* transgene. (del Campo et al., 2005; Shemer et al., 2004). The projection of the z-slices of intestine is shown. Some intestinal cells have fused. Immunofluorescence with anti-EFF-1 antibody (green) and anti-DLG-1 (apical junction, magenta).

(G) Ectopic EFF-1 is detected in the plasma membrane of mammalian BHK cells transfected with *eff-1::*V5 construct (arrows). Immunofluorescence with anti-V5 antibody (green) and DAPI (nuclei, blue).

Scale bar represents 5 μm in (A-D) and 10 μm in (D-F).

Table S1

EFF-1 colocalization with cellular markers, related to Figure 4

Organelle (Ordered from highest to lowest)	**Strain**	**Protein**	**Mean (%) colocalization ±SEM**	**number of puncta**	**number of embryos**
Early endosome (EE)	RT122	RAB-5::GFP	58.2 ± 5.7	1766	21
Early endosome to MVB	DH1336	RME-8::GFP	30.3 ±7.3	436	6
Golgi	RT1315	MANS::GFP	19.2 ± 4.4	278	6
Lysosome	RT258	LMP-1::GFP	8.5 ± 3.3	272	6
Basolateral membrane	BP712	LET-413::CFP	8.3 ± 2.1	460	8
Apical junction	SU93	AJM-1::GFP	6.5 ± 2.3	803	11
Apical junction	N2	DLG-1 (Ab)	6.2 ± 1.7	534	9
Apical endosome	RT311	RAB-11::GFP	3.6 ± 1.5	273	5
EE from Golgi to PM	RT525	RAB-10::GFP	3 ± 0.9	408	5
Recycling endosome	RT348	RME-1::GFP	1.8 ± 0.04	378	5
Late endosome	RT476	RAB-7::GFP	1.9 ± 0.7	198	5
Autophagosome	BU071	LGG-1::GFP	1.7 ± 0.7	224	5
MVB	RT1356	ALX-1::GFP	1 ± 0.6	208	5
Vacuolar ATPase	ML846	VHA-5::GFP	0.9 ± 0.3	321	5
MVB	RT1341	HGRS-1::GFP	0 ± 0.04	98	5
Mitochondria	N2	HSP60-s (Ab)	No (visual observation)	-	12
Proteasome	N2	PAS-7 (Ab)	No (by visual observation)	-	15
ER	N2	CYP33E1-s (Ab)	No (by visual observation)	-	14
Endocytic invagination	N2	DYN-1 (Ab)	No (by visual observation)	-	10

Table S2
Hyperfusion and ectopic EFF-1 expression in trafficking mutants, related to Figure 3

Affected pathway	**Strain**	**Protein mutated (*allele*)**	**Hyperfusion**	**EFF-1 mislocalization to apical junctions**
Retrograde Golgi to ER	RB1535	ARF1.1(*ok1840*)	No	No
Early endocytosis	CX51	DYN-1(*ky51*)	**Yes**	**Yes**
Basolateral recycling	RT2	RAB-10(*q373*)	No	No
Basolateral recycling	VC1026	RAB-10(*ok1494*)	No	No
Recycling	DH1201	RME-1(*b1045*)	No	No
Early, recycling, late endocytosis	DH1206	RME-8(*b1023*)	No	No
Early endocytosis	VC2199	RAB-5(*ok2605*)	**Yes**	**Yes**
RAB-5 regulation	VC1282	RABX-5(*ok1763*)	No	No
Endocytic recycling	RT206	RAB-35(*b1013*)	No	No
Endocytic recycling	VC900	ALX-1(*gk412*)	No	No
To lysosome	GS2643	CUP-5(*ar465*)	No	No
Endosomal acidification, trafficking, apical secretion (V0-ATPase, subunit H)	JR2750	VHA-17/FUS-1(*w13*)	**Yes**	No
Endosomal acidification, trafficking, apical secretion (V0-ATPase, subunit A)	ML851	VHA-5(*mc38*)	**Yes**	No

Table S3
Fusion abnormalities and ectopic EFF-1 expression in embryos treated with RNAi, related to Figure 2

RNAi	Phenotype	Fusion defects in embryos (n)	Fusion defects in larvae (n)	EFF-1 mislocalization
rab-5	emb. lethal	yes (103)	-	yes
dyn-1	emb. lethal	yes (55)	-	yes
aps-1	no	no (45)	no (15)	no
syn-4	no	no (37)	no (10)	no
rab-6.1	no	no (35)	no (22)	no
rab-6.2	no	no (40)	no (15)	no
rme-6	no	no (48)	no (18)	no
rabx-5	no	no (42)	no (20)	no
bli-4 positive control	emb. lethal	no (20)	-	no
C06C3.5 negative control	no	no (20)	no (20)	no

Supplemental movie legends

Movie S1. EFF-1 dynamics during cell fusion, related to Figures 2 and 5
Time lapse recording of an *eff-1(hy21)II; mcIs46[dlg-1::RFP]; hyEx160[peff-1::eff-1::GFP]* transgenic embryo. EFF-1::GFP is shown in green, DLG-1::RFP is displayed in magenta. The z-series were recorded every 15 sec using spinning disk confocal microscopy, multiple intensity projection of a z-stack is shown at each time point. Lower panel represents enlarged area of the embryo (same embryo as in Figure 5). Arrows mark the start of apical junction disassembly. Time in minutes:seconds is shown at the top right corner.

Movie S2. EFF-1::GFP dynamics during late stages in syncytia formation in the dorsal hypodermis, related to Figure 2
Another embryo of an *eff-1(hy21)II; mcIs46[dlg-1::RFP]; hyEx160[peff-1::eff-1::GFP]* strain showing later stages of hypodermis fusion. Arrows indicate the beginning of apical junction disassembly. Microscopy and time interval as in **Movie S1**.

Movie S3. EFF-1 dynamics after RAB-5 depletion by RNAi, related to Figure 2E
Time lapse recording of an *eff-1(hy21)II; mcIs46[dlg-1::RFP]; hyEx160[peff-1::eff-1::GFP]* embryo after *rab-5*(RNAi) treatment. Green represents EFF-1::GFP, magenta shows DLG-1::RFP. The z-series were recorded every 30 seconds, lower panel represents enlarged area of the fusion (**Figure 2E**). Arrow marks the beginning of apical junction disassembly. Note the disappearance of the bright EFF-1::GFP puncta, the localization of EFF-1::GFP on the junctions and the increase of numerous small and less bright EFF-1::GFP vesicular staining.

Movie S4. *rab-5* depletion induces EFF-1 mislocalization to the apical plasma membrane and hyperfusion, related to Figures 2 and S2
Animated z-stack of an *eff-1(hy21)II; mcIs46[dlg-1::RFP]; hyEx160[peff-1::eff-1::GFP]* embryo treated with *rab-5* RNAi. All cells in the dorsal hypodermis are fused to each other (hyperfusion) in contrast to three unfused syncytia (*hyp5, 6,* and 7) in the *wt* embryos (**Figure 1A**). EFF-1 is expressed on plasma membrane of hypodermis syncytia. Maximum intensity projection of the dorsal side of this embryo is shown in Supplemental **Figure S2G, S2H**.

Movie S5. Apical membrane EFF-1 expression and hyperfusion induced by *dyn-1* RNAi, related to Figure 2F
Animated z-stack of live embryo expressing EFF-1::GFP and DLG-1::RFP after *dyn-1* RNAi treatment. This embryo shows EFF-1::GFP expression on the apical membrane, defects in embryogenesis, and hyperfusion.

Movie S6. *rab-5* RNAi depletion induce EFF-1::GFP accumulation to all surrounding apical membranes, related to Figure 6
Time lapse recording of an *eff-1(hy21)II; mcIs46[dlg-1::RFP]; hyEx160[peff-1::eff-1::GFP]* embryo after *rab-5*(RNAi) treatment. Green represents EFF-1::GFP, magenta shows DLG-1::RFP. The z-series were recorded every 30 seconds.

Supplemental experimental procedures

All nematode strains were maintained according to standard protocols (Brenner, 1974; Sulston and Hodgkin, 1988). In addition to the wild-type strain N2, the following mutations, transgenes and strains were used:

Markers of cell junctions and cytoskeleton

SU93	*jcIs1[ajm-1::gfp; unc-29(+); rol-6(su1006)]*	CGC; (Mohler et al., 1998)
ML1651	*mcIs46 [dlg-1::rfp; unc-119(+)]*	Michel Labouesse; (Diogon et al., 2007)
	let-413::cfp; rol-6	Olaf Bossinger; (Pilipiuk et al., 2009)
CZ3464	*ifb-1::gfp*	Limor Broday; (Woo et al., 2004)

EFF-1 alleles

BP75	*eff-1(hy21)II*	BP; (Mohler et al., 2002)
BP347	*eff-1(ok1021)II*	BP; (Podbilewicz et al., 2006)

Markers of intracellular organelles

DH1336	*bIs34[rme-8::GFP + rol-6(su1006)]*	CGC; (Zhang et al., 2001)
RT122	*pwIs20[GFP::rab-5 + unc-119(+)]*	CGC; (Sato et al., 2005)
RT311	*pwIs69[vha6p::GFP::rab-11 + unc-119(+)]*	CGC; (Chen et al., 2006)
RT476	pwIs170[*vha6p::GFP::rab-7 + Cb unc-119(+)]*	CGC; (Chen et al., 2006)
RT525	pwIs206[*vha6p::GFP::rab-10 + Cb unc-119(+)]*	CGC; (Chen et al., 2006)
RT1043	pwIs403[*Ppie-1::mCherry::rab-5 + unc-119(+)]*	CGC; (Sato et al., 2008)
RT1315	pwIs481[*Pvha-6::mans::GFP]*	CGC; (Chen et al., 2006)
RT258	pwIs50[*lmp-1::GFP + Cb-unc-119(+)]*	CGC; (Treusch et al., 2004)
DA2123	*Plgg-1;GFP::LGG-1;rol-6*	Hong Zhang; (Melendez et al., 2003)
RT1356	*pwIs524 (pvha-6::GFP::ALX-1)*	Barth Grant; (Shi et al., 2007)
RT4	*pwIs1 (palx-1::GFP::ALX-1)*	Barth Grant; (Shi et al., 2007)
RT1341	*pwIs518 (pvha-6::GFP::HGRS-1)*	Barth Grant; (Shi et al., 2007)
RT348	*pwIs87 (pvha-6::GFP::RME-1)*	Barth Grant; (Shi et al., 2007)
ML846	*vha-8(mc38)IV; mcEx337[vha-5(+)::GFP; rol-6(su1006)]*	CGC; (Liegeois et al., 2006)

Traffic mutants

CX51	*dyn-1(ky51) X*	CGC; (Clark et al., 1997)
VC900	*alx-1(gk412) III.*	CGC; (Shi et al., 2007)
RT2	*rab-10(q373) I*	CGC; (Chen et al., 2006)
DH1201	*rme-1(b1045) V.*	CGC; (Shi et al., 2007)
VC1026	*rab-10(ok1494) I.*	CGC; (Shi et al., 2012)
RB1535	*arf-1.1&F45E4.7(ok1840) IV*	CGC; (Sato et al., 2014)
ML732	*vha-5(mc38)/unc-24(e138) dpy-20(e1282) IV*	CGC; (Liegeois et al., 2006)
JR2750	*vha-17/fus-1(w13)*	Joel Rothman; (Kontani et al., 2005)
VC2199	*rab-5(ok2605) I/hT2[bli-4(e937) let-?(q782) qIs48](I;III)*	CGC; (Sato et al., 2014)
DH1206	*rme-8(b1023) I*	CGC; (Zhang et al., 2001)
VC1282	*rabx-5(ok1763) III*	CGC; (Sato et al., 2005)
RT206	*rab-35(b1013) III*	Barth Grant; unpublished

Strains constructed in this study:

BP953	*eff-1(hy21)II; mcIs46 [dlg-1::rfp; unc-119(+)]*	BP; this study
BP954	*eff-1(hy21)II; mcIs46; hyEx160[peff-1::eff-1::GFP]*	BP; this study
BP955	*rab-5(ok2605) I/hT2[bli-4(e937) let (q782) qIs48](I;III); mcIs46*	BP; this study
BP956	*rab-5(ok2605) I/hT2[bli-4(e937) let(q782) qIs48](I;III); eff-1(hy21)II; mcIs46[dlg-1::rfp; unc-119(+)]*	BP; this study

Immunofluorescence of *C. elegans* embryos

Eggs were collected by hypochlorite treatment of gravid adult worms and transferred to poly-lysine coated slides. Embryos were permeabilized by the freeze-crack method (Strome and Wood, 1983) and fixed in 100% methanol (5 min), 100% acetone (5 min) at -20°C. Slides were washed for 10 min with PBS, and blocked with blocking solution of 0.2% Ez-Block (Biological Industries, Israel) in PBST (PBS with 0.01% Tween). Slides were incubated for 1 h at room temperature with primary antibodies, washed three times for 10 min each with PBS at room temperature, and incubated at room temperature for 1 h with Alexa488, Alexa568, or Alexa647 conjugated α-mouse or α-rabbit secondary antibodies (Molecular Probes) in PBST. Slides were washed three times for 10 min each in PBST and mounted in Fluoromount-G (Southern Biotech). The following primary antibodies were used at the dilutions indicated: α-EFF-1 (ascites 20.10 from mouse; at 1:1000; Fridman et al., Submitted); MH27 (α-AJM-1, mouse, at 1: 500), α-GFP (rabbit; 1:500; MBL), α-tubulin (mouse, Sigma, 1:500). α-DLG-1 antibody (rabbit, at 1:400) is a kind gift from Olaf Bossinger. MH46 (α-myotactin, mouse, at 1: 400) is a kind gift from Limor Broday, Antibodies against C. elegans proteins CYP33E1-s, PAS-7, HSP60-s were obtained from Developmental Studies Hybridoma Bank (Hadwiger et al., 2010) and used in 1:10 dilution. Texas-red X phalloidin (Molecular probes) in final concentration of 0.2 µM was added with secondary antibody.

Cell culture, live imaging and immunofluorescence of BHK cells

Baby Hamster Kidney (BHK) cells and their growth conditions were according to standard protocols (Stoker and Macpherson, 1964). Cells were grown in Dulbecco's Modified Eagle's Medium (DMEM, Gibco) supplemented with 10% Fetal Bovine Serum, 2 mM L-Glutamine, 100 µg/ml Penicillin and 100 µg/ml streptomycin (Biological Industries, Kibbutz Beit Haemek, Israel) and sodium pyruvate (Gibco) in a humid atmosphere of 5% CO2 up to a maximal density of 10^6/ml. Cells were transfected with 2 µg/ml of *eff-1* pCAGGS DNA vector using Fugene 6 (Roche) at 1:4 ratio. After 24 hours of transfection the cells were fixed with 4% paraformaldehyde in PBS and

processed for immunofluorescence. Cells were incubated in 40 mM NH4Cl, washed in PBS, permeabilized in 0.1% tritonX-100 in PBS and blocked in 1% FBS in PBS. The coverslips were incubated 1 hour with anti-V5 1:500 (Invitrogen) mouse monoclonal antibodies at RT. The secondary antibodies were goat anti-mouse coupled to Alexa488 (Molecular Probes/Invitrogen), nuclei were visualized with DAPI (1 μg/ml) (Avinoam et al., 2011; Perez-Vargas et al., 2014).

Supplemental references

Avinoam, O., Fridman, K., Valansi, C., Abutbul, I., Zeev-Ben-Mordehai, T., Maurer, U.E., Sapir, A., Danino, D., Grunewald, K., White, J.M.*, et al.* (2011). Conserved eukaryotic fusogens can fuse viral envelopes to cells. Science *332*, 589-592.

Brenner, S. (1974). The genetics of Caenorhabditis elegans. Genetics *77*, 71-94.

Chen, C.C., Schweinsberg, P.J., Vashist, S., Mareiniss, D.P., Lambie, E.J., and Grant, B.D. (2006). RAB-10 is required for endocytic recycling in the Caenorhabditis elegans intestine. Mol Biol Cell *17*, 1286-1297.

Clark, S.G., Shurland, D.L., Meyerowitz, E.M., Bargmann, C.I., and van der Bliek, A.M. (1997). A dynamin GTPase mutation causes a rapid and reversible temperature-inducible locomotion defect in C. elegans. Proc Natl Acad Sci U S A *94*, 10438-10443.

del Campo, J.J., Opoku-Serebuoh, E., Isaacson, A.B., Scranton, V.L., Tucker, M., Han, M., and Mohler, W.A. (2005). Fusogenic activity of EFF-1 is regulated via dynamic localization in fusing somatic cells of C. elegans. Curr Biol *15*, 413-423.

Diogon, M., Wissler, F., Quintin, S., Nagamatsu, Y., Sookhareea, S., Landmann, F., Hutter, H., Vitale, N., and Labouesse, M. (2007). The RhoGAP RGA-2 and LET-502/ROCK achieve a balance of actomyosin-dependent forces in C. elegans epidermis to control morphogenesis. Development *134*, 2469-2479.

Gattegno, T. (2003). Isolation and characterization of cell-fusion mutants in C. elegans. In Biology (Technion).

Hadwiger, G., Dour, S., Arur, S., Fox, P., and Nonet, M.L. (2010). A monoclonal antibody toolkit for C. elegans. PLoS One *5*, e10161.

Kontani, K., Moskowitz, I.P., and Rothman, J.H. (2005). Repression of cell-cell fusion by components of the C. elegans vacuolar ATPase complex. Dev Cell *8*, 787-794.

Liegeois, S., Benedetto, A., Garnier, J.M., Schwab, Y., and Labouesse, M. (2006). The V0-ATPase mediates apical secretion of exosomes containing Hedgehog-related proteins in Caenorhabditis elegans. J Cell Biol *173*, 949-961.

Melendez, A., Talloczy, Z., Seaman, M., Eskelinen, E.L., Hall, D.H., and Levine, B. (2003). Autophagy genes are essential for dauer development and life-span extension in C. elegans. Science *301*, 1387-1391.

Mohler, W.A., Shemer, G., del Campo, J.J., Valansi, C., Opoku-Serebuoh, E., Scranton, V., Assaf, N., White, J.G., and Podbilewicz, B. (2002). The type I membrane protein EFF-1 is essential for developmental cell fusion. Dev Cell *2*, 355-362.

Mohler, W.A., Simske, J.S., Williams-Masson, E.M., Hardin, J.D., and White, J.G. (1998). Dynamics and ultrastructure of developmental cell fusions in the Caenorhabditis elegans hypodermis. Curr Biol *8*, 1087-1090.

Perez-Vargas, J., Krey, T., Valansi, C., Avinoam, O., Haouz, A., Jamin, M., Raveh-Barak, H., Podbilewicz, B., and Rey, F.A. (2014). Structural basis of eukaryotic cell-cell fusion. Cell *157*, 407-419.

Pilipiuk, J., Lefebvre, C., Wiesenfahrt, T., Legouis, R., and Bossinger, O. (2009). Increased IP3/Ca2+ signaling compensates depletion of LET-413/DLG-1 in C. elegans epithelial junction assembly. Dev Biol *327*, 34-47.

Podbilewicz, B., Leikina, E., Sapir, A., Valansi, C., Suissa, M., Shemer, G., and Chernomordik, L.V. (2006). The C. elegans developmental fusogen EFF-1 mediates homotypic fusion in heterologous cells and in vivo. Dev Cell *11*, 471-481.

Sato, K., Norris, A., Sato, M., and Grant, B.D. (2014). C. elegans as a model for membrane traffic. WormBook, 1-47.

Sato, M., Sato, K., Fonarev, P., Huang, C.J., Liou, W., and Grant, B.D. (2005). Caenorhabditis elegans RME-6 is a novel regulator of RAB-5 at the clathrin-coated pit. Nat Cell Biol *7*, 559-569.

Sato, M., Sato, K., Liou, W., Pant, S., Harada, A., and Grant, B.D. (2008). Regulation of endocytic recycling by C. elegans Rab35 and its regulator RME-4, a coated-pit protein. Embo j *27*, 1183-1196.

Shemer, G., Suissa, M., Kolotuev, I., Nguyen, K.C., Hall, D.H., and Podbilewicz, B. (2004). EFF-1 is sufficient to initiate and execute tissue-specific cell fusion in C. elegans. Curr Biol *14*, 1587-1591.

Shi, A., Liu, O., Koenig, S., Banerjee, R., Chen, C.C., Eimer, S., and Grant, B.D. (2012). RAB-10-GTPase-mediated regulation of endosomal phosphatidylinositol-4,5-bisphosphate. Proc Natl Acad Sci U S A *109*, E2306-2315.

Shi, A., Pant, S., Balklava, Z., Chen, C.C., Figueroa, V., and Grant, B.D. (2007). A novel requirement for C. elegans Alix/ALX-1 in RME-1-mediated membrane transport. Curr Biol *17*, 1913-1924.

Stoker, M., and Macpherson, I. (1964). SYRIAN HAMSTER FIBROBLAST CELL LINE BHK21 AND ITS DERIVATIVES. Nature *203*, 1355-1357.

Strome, S., and Wood, W.B. (1983). Generation of asymmetry and segregation of germ-line granules in early C. elegans embryos. Cell *35*, 15-25.

Sulston, J., and Hodgkin, J. (1988). Methods. In The Nematode Caenorhabditis elegans, W.B. Wood, ed. (Cold Spring Harbor: Cold Spring Harbor Laboratory), pp. 587-606.

Treusch, S., Knuth, S., Slaugenhaupt, S.A., Goldin, E., Grant, B.D., and Fares, H. (2004). Caenorhabditis elegans functional orthologue of human protein h-mucolipin-1 is required for lysosome biogenesis. Proc Natl Acad Sci U S A *101*, 4483-4488.

Woo, W.M., Goncharov, A., Jin, Y., and Chisholm, A.D. (2004). Intermediate filaments are required for C. elegans epidermal elongation. Dev Biol *267*, 216-229.

Zhang, Y., Grant, B., and Hirsh, D. (2001). RME-8, a conserved J-domain protein, is required for endocytosis in Caenorhabditis elegans. Mol Biol Cell *12*, 2011-2021.